

Prediction and predictability of a catastrophic local extreme precipitation event through cloud-resolving ensemble analysis and forecasting with Doppler radar observations

QIU XueXing^{1,2*} & ZHANG FuQing²

¹Anhui Meteorological Observatory, Hefei 230031, China;

²Department of Meteorology, Pennsylvania State University, University Park, PA 16802, USA

Received May 29, 2015; accepted September 29, 2015; published online December 17, 2015

Abstract Local extreme rain usually resulted in disasters such as flash floods and landslides. Upon today, it is still one of the most difficult tasks for operational weather forecast centers to predict those events accurately. In this paper, we simulate an extreme precipitation event with ensemble Kalman filter (EnKF) assimilation of Doppler radial-velocity observations, and analyze the uncertainties of the assimilation. The results demonstrate that, without assimilation radar data, neither a single initialization of deterministic forecast nor an ensemble forecast with adding perturbations or multiple physical parameterizations can predict the location of strong precipitation. However, forecast was significantly improved with assimilation of radar data, especially the location of the precipitation. The direct cause of the improvement is the buildup of a deep mesoscale convection system with EnKF assimilation of radar data. Under a large scale background favorable for mesoscale convection, efficient perturbations of upstream mid-low level meridional wind and moisture are key factors for the assimilation and forecast. Uncertainty still exists for the forecast of this case due to its limited predictability. Both the difference of large scale initial fields and the difference of analysis obtained from EnKF assimilation due to small amplitude of initial perturbations could have critical influences to the event's prediction. Forecast could be improved through more cycles of EnKF assimilation. Sensitivity tests also support that more accurate forecasts are expected through improving numerical models and observations.

Keywords EnKF, Doppler radar data, Local extreme rain, Predictability

Citation: Qiu X X, Zhang F Q. 2016. Prediction and predictability of a catastrophic local extreme precipitation event through cloud-resolving ensemble analysis and forecasting with Doppler radar observations. *Sci China Earth Sci*, 59: 518–532, doi: 10.1007/s11430-015-5224-1

1. Introduction

Local extreme rain usually resulted in disasters such as flash floods, landslides and urban waterlogging, causing great loss of human lives and properties. Despite of the strong demand for accurate forecast and early warning for these events from our community, it is still one of the most difficult tasks to make accurate forecast of these extreme events

for operational forecast centers.

Many previous studies showed local extreme rain is closely related to mesoscale or small scale weather system (Schumacher and Johnson, 2005, 2006; Zhang et al., 2014). Among all available observations, Doppler radar scanning is one of the most important ways for measurement of meso- and small-scale weather systems, thus effective assimilation of these Doppler radar observations has become a major research focus. After Snyder et al. (2003) first demonstrated the potential applications of ensemble Kalman filter (EnKF) assimilation of Doppler radar data, great progress has been

*Corresponding author (email: qiu Xuexing@126.com)

made with this approach on regional model data assimilation. Dowell et al. (2004) started to use EnKF to assimilate real-time radar data, and successfully retrieved the wind and temperature fields. EnKF assimilation of radar data has also been used to improve the initial fields of the several numerical models including but not limited to the ARPS model (Tong and Xue, 2005; Xue et al., 2006; Lan et al., 2010a, 2010b), a three-dimension cloud model (Xu et al., 2006) and the WRF model (Aksoy et al., 2009, 2010; Min et al., 2011). Experiments from these models proved positive impacts of EnKF assimilation of radar data on numerical forecasts. EnKF is also successfully applied on assimilation of airborne radar observations (Zhang et al., 2009a; Weng and Zhang, 2012) that showed hurricane intensity forecast was significantly improved. For 2–4 days forecasts, the intensity of the storm can be improved by 25%–28% averaged over 100 cases they studied (Zhang and Weng, 2015). All the above results suggested EnKF assimilation of radar observations can improve the initial fields for numerical models and ultimately improve the model performance.

Besides the initial fields, performance of numerical models on forecasting local extreme rain also depends on intrinsic predictability of individual weather system. Zhang et al. (2006a) analyzed the predictability of an extreme rain event in the central US, their results showed the small errors of small scale initial fields will grow rapidly and cascade up-scale, and finally impact forecast. Simulation of Mei-yu front precipitation has similar aspects. The growth rate of initial analysis error varies with its spatial scale (Bei and Zhang, 2007). Liu et al. (2009) divided the growth of initial error to amplitude growing, scale growing and amplitude re-growing. Initial errors from different variables also impact differently on the heavy rain forecast. Zhu et al. (2009) found that heavy rainfall during pre-flood season of southern China is more sensitive to the errors of initial temperature fields. When initial fields generated by EnKF analysis was used in numerical models, the difference of assimilation will influence its predictability. Previous studies about the predictability mainly focus on extended-range precipitation where data assimilation of radar observations was rarely included. Very few studies have been carried out on small scale local extreme rain cases, and each of these cases has their own development mechanisms and background. In this paper, a local extreme rain case was studied. WRF model with EnKF assimilation of Doppler radar radial velocity was conducted to simulate its mesoscale evolution, and analyze the predictability of this extreme case. We hope this paper will provide reference for future improvement of forecast on this kind of extreme cases.

2. Case description

This extreme rain event occurred on June 30, 2013 (from 00Z to 06Z, UTC) in the south of Anhui province, China.

Figure 1 showed 6-h accumulated rainfall. “x” marks the location of Doppler radar (Huangshan station, 118.15°E, 30.13°N, elevation 1841 m). Heavy rainfall is mainly located to the east and south of the radar. The maximum rainfall observed at automatic weather station (AWS) is 185.3 mm, heavy rainfall over 50 mm concentrated within an area of 0.5°×0.5°. This extreme rain event impacted only a very small region, however, because it occurred in the southern mountain area of Anhui, mountain flash flood and landslides are triggered and 12 casualties are recorded. According to the radar reflectivity map (figure not shown), at 19Z June 29, weak precipitation echo can be noticed at 100 km to the west of the radar and moved eastward. This weak precipitation echo approached to the radar location and arrived around 00Z June 30. After that, the echo intensified and persisted around to the east and south of the radar station which resulted in this extreme event.

This case occurred in the northwest of western North Pacific subtropical high. Synoptic configurations are showed in Figure 2. Southwest flow in the northwest of the subtropical high bring warm and moist air which builds up an unstable stratification, when combined with an eastward moving low level jet, creates a favorable condition for convection. More specifically, at 500 hPa, this region is to the right of the ridge where northwest winds dominated, strong vertical wind shears provided a favorable condition for this extreme event. At 00Z June 30 (Figure 2(a)), a low level jet with wind speed over 14 m/s at 850 hPa is upstream of the extreme rain, and the extreme rain occurs in the exit region of the low level jet. Wind convergence is likely the trigger of this extreme rain. The core of the low level jet moved eastward along the edge of subtropical high. Upon 06Z (Figure 2(b)), the low level jet moved to the east of the extreme rain. This region by this time is now at the entrance of the jet, which is no longer a favorable condition, heavy rain gradually dissipated.

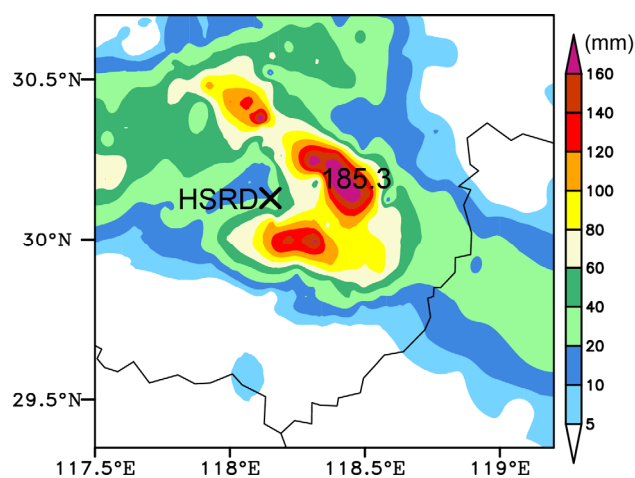


Figure 1 6-hour (00Z-06Z) observed rainfall on June 30, “x” represents the location of radar (Huangshan station).

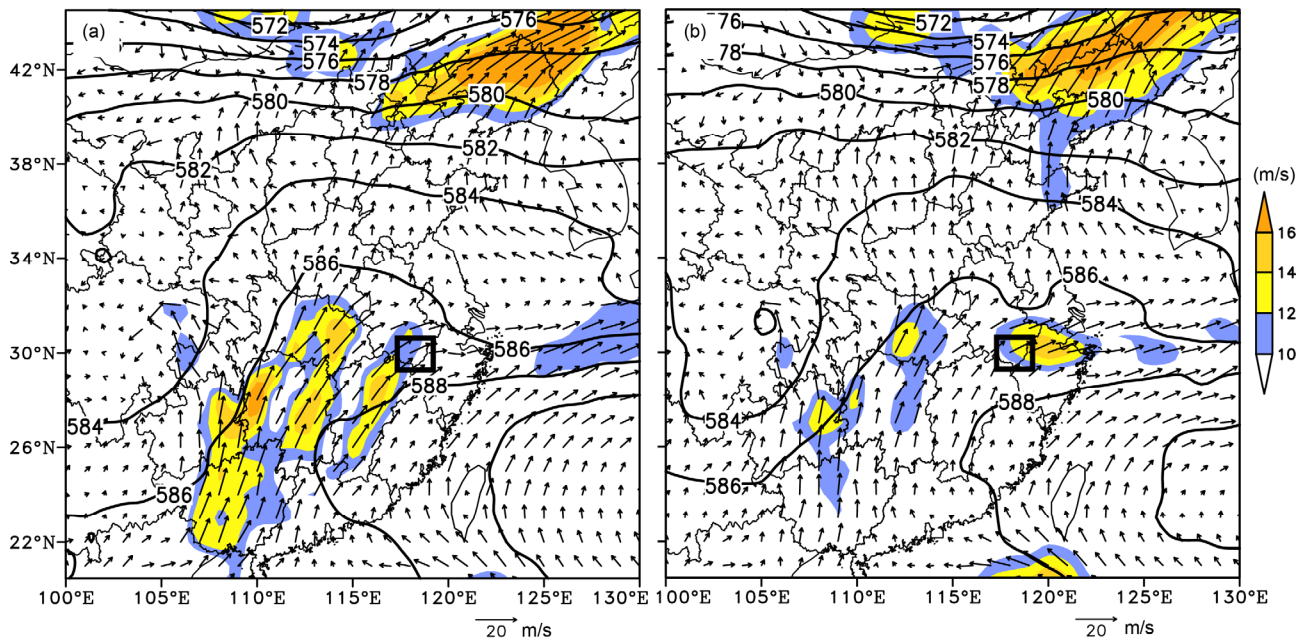


Figure 2 500 hPa geopotential heights and 850hPa wind (wind speed is shaded, unit m/s) at 00Z (a) and 06Z (b) on June 30. The square with thick line represents the extreme rain region.

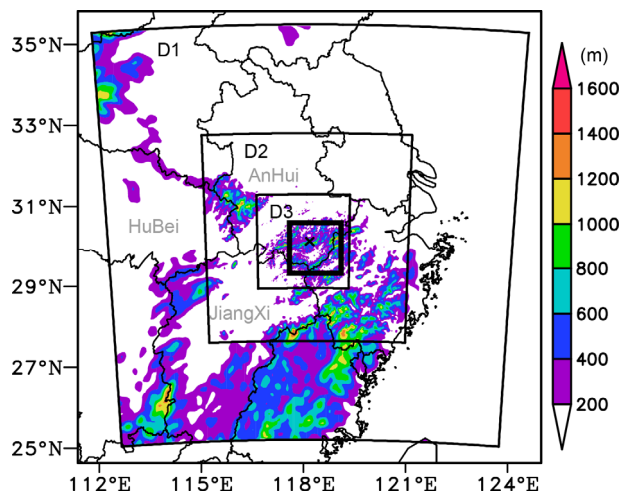


Figure 3 WRF model nested domains (terrain is shaded). The square with thick line represents the extreme rain region.

3. Assimilation system and experimental design

3.1 Assimilation method and forecast model

In this paper, we use the WRF-based EnKF system developed at the Pennsylvania State University (PSU-EnKF) (Zhang et al., 2006b; Meng and Zhang, 2007, 2008a, 2008b; Zhang et al., 2009a) to assimilate Doppler radar data. The forecast model is WRFV3.6 (Skamarock et al., 2008). Three nested domains are used with horizontal resolutions are 9, 3 and 1 km and grid points are 129×129 , 262×262 and 262×262 respectively (Figure 3). There are 35 vertical levels, and the top level is set to 50 hPa. We use 36 ensemble members for this study. We first use the WRFDA “cv3”

option from background error covariance (Barker et al., 2004) to generate the initial perturbations at 12Z June 29 for domain 1, and then use the WRF model to downscale the initial perturbations to domain 2 and domain 3. We assimilate observations at each model level hourly with assimilation window from 18Z June 29 to 00Z June 30. To avoid far small dispersion of ensemble forecast, we use the inflation through relaxation method for background error covariance introduced in Zhang et al. (2004), and set the weight as 0.5. Multiple physical parameterization schemes have been used to represent the uncertainties of the model in previous studies (Meng and Zhang, 2007; Lan et al., 2010b); we follow previous approaches and use random combination of multiple physical parameterization schemes in this study. After assimilation of observations at 00Z June 30, we use the EnKF ensemble mean analysis and analysis of individual ensemble members for 6-hour deterministic forecast (DF) and ensemble forecast (EF). For all the experiments, we use the same parameterization schemes for deterministic forecast. The WSM6 scheme for microphysics (Hong et al., 2004), the YSU scheme for boundary layer (Noh et al., 2003) and the explicit scheme for cumulus parameterizations are used.

3.2 Initial fields, boundary conditions and observations

The initial and boundary condition data are obtained from the NCEP $1^\circ \times 1^\circ$ reanalysis data, including surface and 26 vertical pressure levels (<http://rda.ucar.edu/datasets/ds083.2>). We use the same method to produce perturbations for lateral boundaries and initial fields.

The observations assimilated with EnKF include regular surface observations and Doppler radar radial velocity data. The quality control and data thinning method from Zhang et al. (2009b) on radar data was applied. For each angle, discrete data of 5 km resolution in the radial direction and 5 degree resolution in the tangential direction was obtained. Observation error of radial velocity was set as 3 m/s for assimilation. The Successive Covariance Localization (SCL) technique of Zhang et al. (2009a) is also adopted for assimilation radar observations. As different localization radius of influence (ROI) is usually used for acquiring information of different scale weather systems from radar observations. A ROI of 405, 135 and 45 km was used to assimilate radar observations of 1/9, 2/9 and 6/9, respectively. Ensemble square root filter (EnSRF, Whitaker and Hamill, 2002; Tippett et al., 2003) was used in the PSU-EnKF system, and observations assimilated with a random sequence were used in this paper.

3.3 Experiments design

The purpose of this study is to analyze the impact of EnKF assimilation of radar observations on the model forecast of this extreme event and assess its predictability. The following six numerical experiments were conducted (Table 1). Figure 4 showed the flow chart of all these experiments. The results of experiments with assimilation of different elevation angles showed the deterministic forecast initia-

lized from the analysis with assimilation of only the lowest two elevation angles (0.5 and 1.5) is the best among all the experiments, therefore this experiment was set as the control experiment (CNTL) for further comparison and discussion. We will focus on analyzing the improvement of forecast on this extreme rain due to assimilation of radar observations and evaluating its predictability. For comparison convenience, NoDA experiment is initialized with 12Z June 29 NCEP FNL reanalysis data and WRF-DA generated initial perturbations for deterministic forecast and ensemble forecast respectively. The model is integrated to 06Z June 30 without assimilation of any observations. Initialization with different perturbations and analysis at 12Z June 29, IP0.5 and CycDA experiments are used to analyze the impacts on numerical model from initial conditions. We also conducted CNTL0.5 and CNTL0.1 experiments for assessing the intrinsic predictability of this case. CNTL0.5 and CNTL0.1 are experiments that the differences between ensemble members and ensemble mean were reduced to 1/2 and 1/10, but the same ensemble mean field with CNTL experiment was used.

4. Results

4.1 Impact of radar observations assimilation with EnKF

First of all, we examine the analysis fields and deterministic

Table 1 Summary of the experiments

Experiments	Description	Purpose
NoDA	No data assimilation	
CNTL	Assimilation the lowest two elevation angles	Impact of EnKF assimilation of radar observations
IP0.5	Same with CNTL, reduce the initial perturbation by 50%	Influence of initial perturbation
CycDA	Initial perturbation and analysis from previous 24h EnKF	EnKF cycling
CNTL0.5	Reduce spread to 1/2	Intrinsic predictability
CNTL0.1	Reduce spread to 1/10	Intrinsic predictability

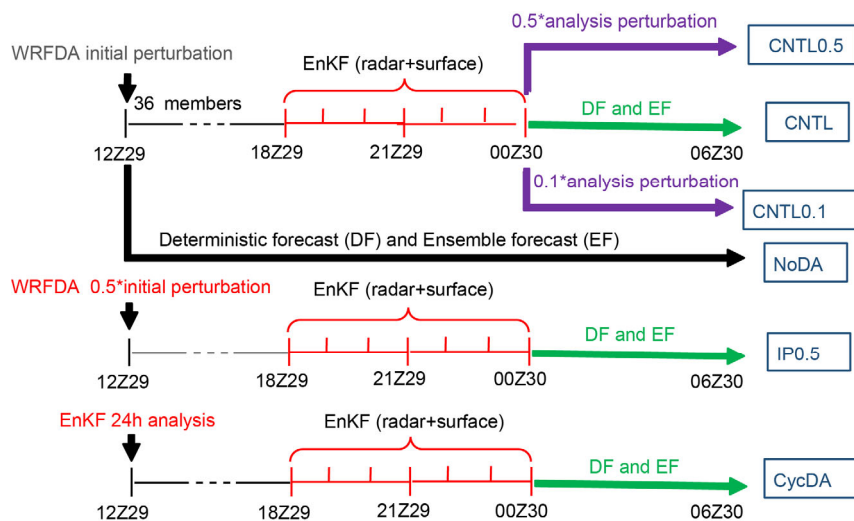


Figure 4 Flow chart of all the experiments.

forecast of the CNTL experiment. In general, EnKF analysis fields shall represent the best estimate of the state of the current atmosphere. It has the smallest analysis error compared with all of the ensemble members. Deterministic forecast made from the initialized fields obtained with the EnKF analysis represents the maximum probability of the atmosphere evolution. Figure 5 shows comparison of composite reflectivity between the observations and analysis of CNTL and NoDA experiments at 00Z June 30, as well as verification of 2 hours forecasts. At 00Z June 30 (Figure 5(a), (b)), despite some small differences of reflectivity in detail, a northwest-southeast echo band can be found over the radar with EnKF assimilation of 6 hours radar observations, which is consistent with observations that a stronger echo to the north and a weaker echo to the south. At 02Z June 30 (Figure 5(d), (e)), deterministic forecast predicted the intensification trend of the echo to the south accurately. Though it also predicted the dissipated echo to the north which did not match the observations, compared with NoDA experiment (Figure 5(c), (f)), forecast improvement is obvious with EnKF assimilation of radar data.

Figure 6 shows the 700 hPa wind analysis in different experiments. For CNTL, there is northwest-southeast me-

ridional wind convergence zone which is collocated with an echo on the composite reflectivity map. This convergence zone remains in the area which is favorable for rainfall accumulation. Also, the positive vorticity advection near the exit of the low level jet probably is another favorable condition. As for the NoDA experiment, there is clear meridional wind convergence at the south and west of the radar station. The convergence at the south and west correspond to the current strong echo (Figure 6(c)) and future strong echo (Figure 6(f)), respectively. The results suggested that EnKF assimilation of radar radial velocity observation is beneficial to improving the location information of the weather systems in the analysis fields.

For the 6-hour rainfall forecast (Figure 7), without assimilation of radar observations (Figure 7(a)), the forecasted rainfall location deviates to the south with 0.5 degree latitude distance. It adjusts to the north (Figure 7(d)) with assimilation of radar data, only 0.1 degree latitude south of the observed location. The predicted maximum rainfall from deterministic forecast is 179.3 mm, close to the observations (185.3 mm) (Figure 1). Ensemble forecast has similar improvement. For the NoDA experiment, (Figure 7(b), (d)), predicted rainfall from the ensemble mean is less than that in observations, the heaviest rainfall deviated to the south of

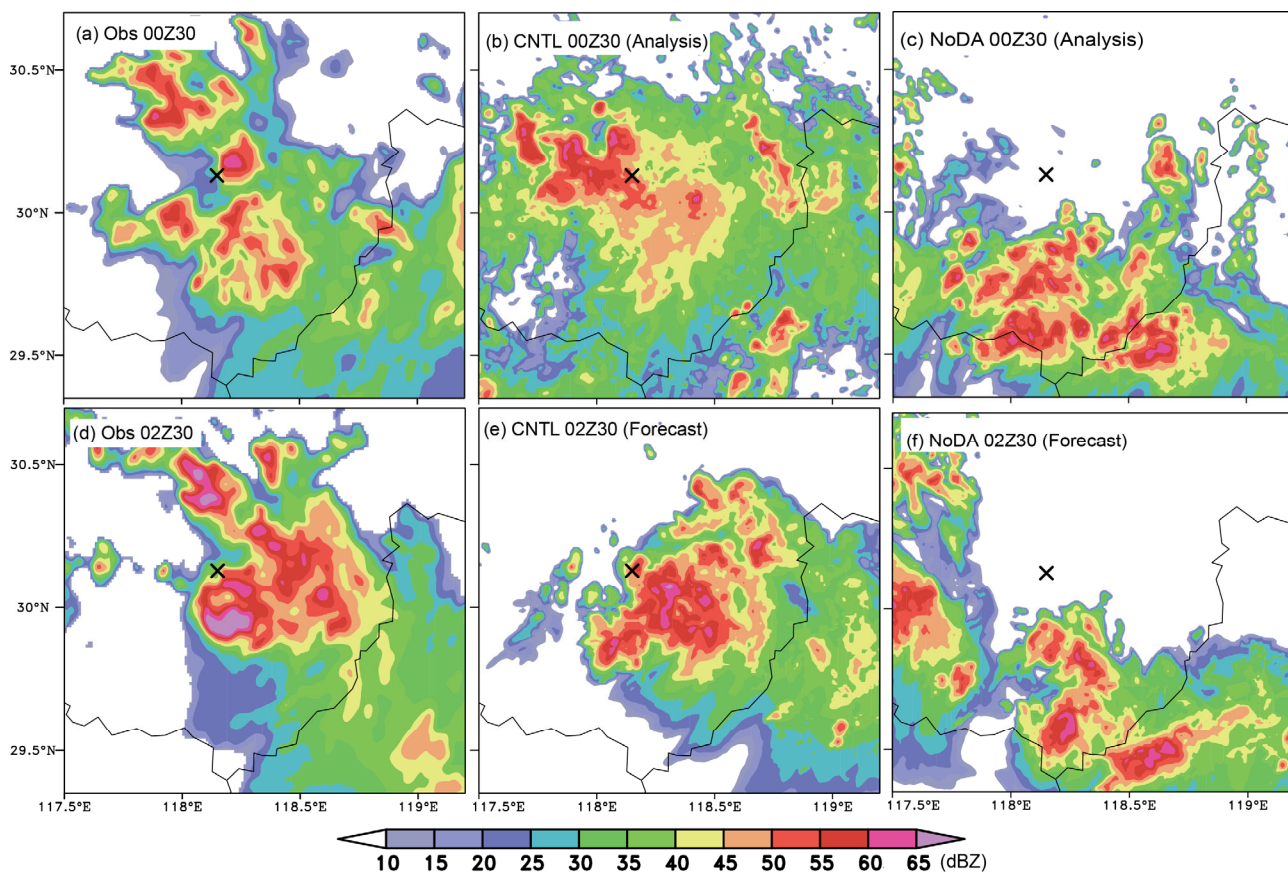


Figure 5 Composite reflectivity at 00Z ((a)–(c)) and 02Z ((d)–(f)) on June 30. (a) and (d) are observations. (b) and (c) are CNTL and NoDA. (e) and (f) are 2-hour deterministic forecast of CNTL and NoDA.

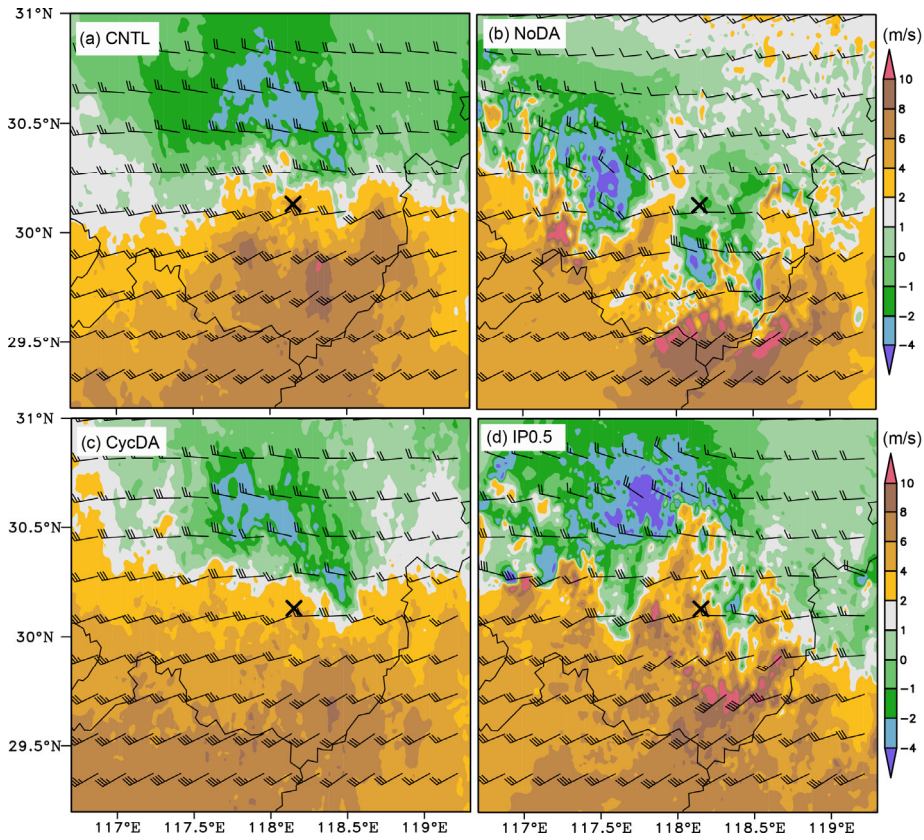


Figure 6 700 hPa meridional wind (shaded) and total wind fields (wind barbs, 4 m/s for each barbs) at 00Z on June 30, 2013 for (a) CNTL (b) NoDA (c) CycDA and (d) IP0.5.

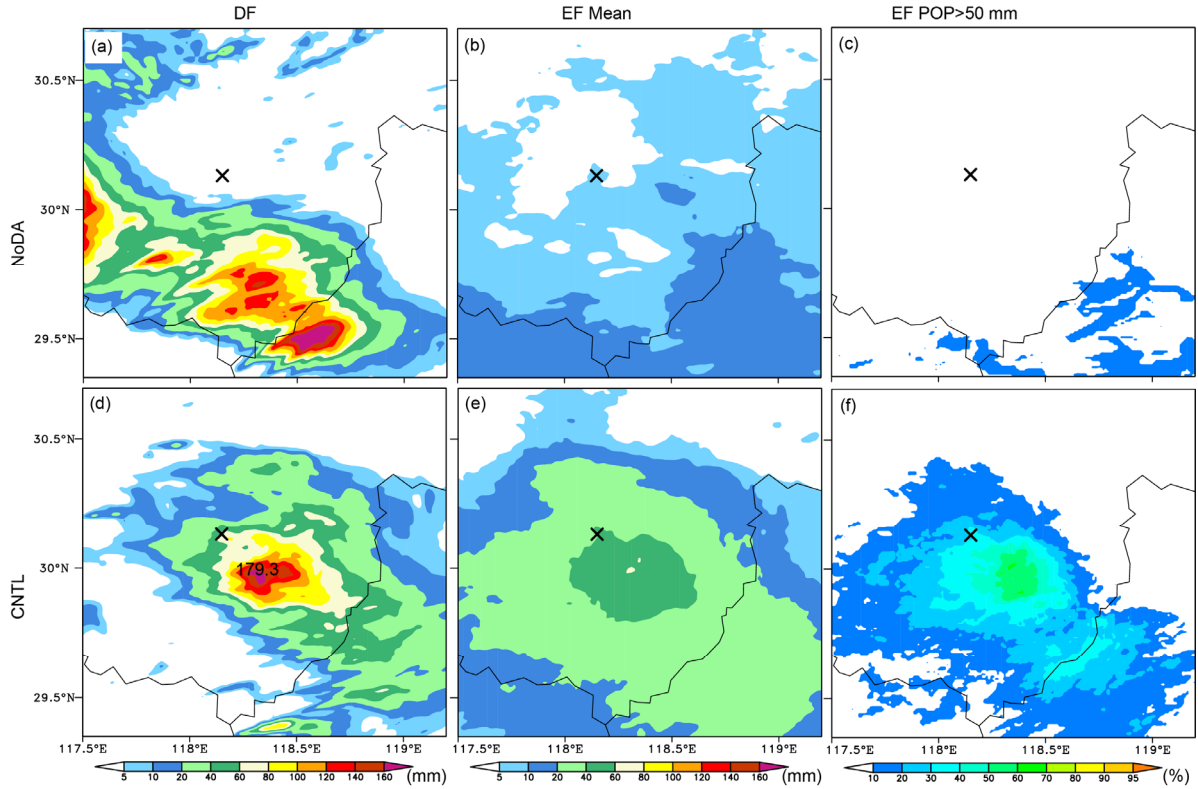


Figure 7 6-hour (from 00Z to 06Z on June 30, 2013) accumulated rainfall from deterministic forecast ((a), (d)) and ensemble mean ((b), (e)). The probability forecast for rainfall over 50 mm is showed in ((c), (f)). The top panel is for NoDA experiment, the bottom panel is for CNTL experiment.

the observations, with magnitude of less than 20 mm. Probability forecast show less than 20% of members forecasted southern rainfall over 50 mm. Compared with NoDA, predicted rainfall from CNTL (Figure 5(e), (f)) is more close to observations, with maximum rainfall of 60 mm, and nearly 50% members forecasted heavy rainfall over 50 mm around the observed rainfall location. Therefore, ensemble forecast approach by adding turbulence in the large scale analysis fields failed to improve the forecast for this specific extreme case. However, with EnKF assimilation of radar radial velocity observations, “ingesting” the high resolution infor-

mation from radar scanning, model forecast can be efficiently improved. Figure 8 ((d)–(f)) shows rainfall forecast from ensemble members (6, 18, 20) whose forecasts are more close to observations. Compared with the NoDA experiment (Figure 8(a)–(c)), rainfall forecasts of all these three members in CNTL are improved. Rainfall forecasts from all the ensemble members (figure not shown) suggest that, even with EnKF assimilation of radar observations, only few members can forecast the magnitude and location of the heavy rainfall correctly, uncertainties still exist for the prediction of this kind of extreme events.

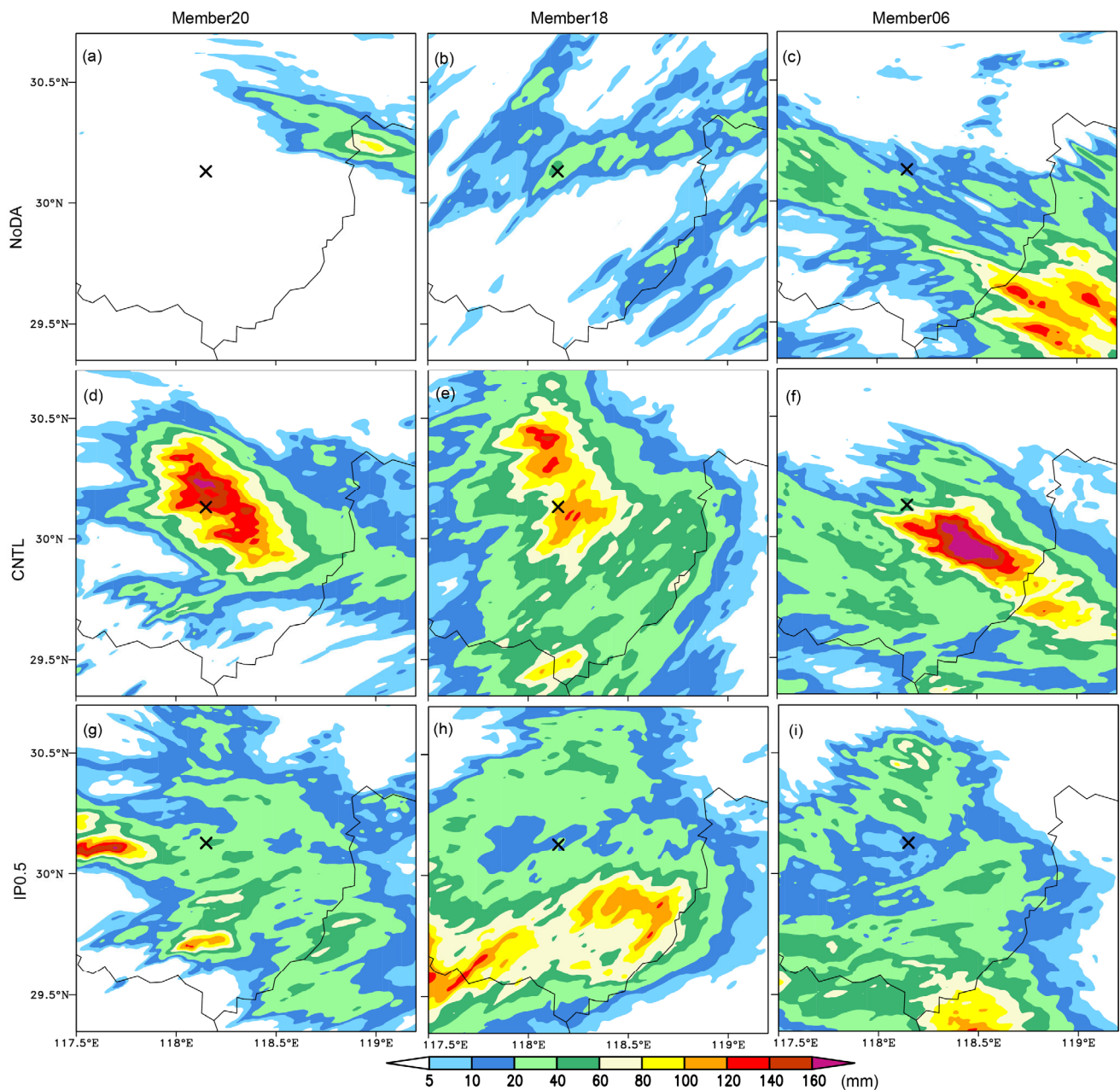


Figure 8 Comparison of 6-hour (00Z-06Z on June 30, 2013) forecasted rainfall from member 20, member 18 and member 6 in different experiments (NoDA, CycDA and IP0.5).

4.2 Analysis of prediction results through ensemble forecast

Ensemble forecast not only can reflect the uncertainties of the forecast, the differences among the ensemble members can provide information for analyzing the factors critical for a successful prediction. With ensemble forecast results of the CNTL experiment, we followed previous studies (Sippel and Zhang, 2008, 2010; Sippel et al., 2011) to calculate the correlations between 6-hour domain-averaged rainfall and several meteorological parameters (from 36 ensemble members). The correlations with coefficients greater than 0.3 and 0.4 are statistical significant with 95% and 99% confidence interval respectively.

We firstly calculated the correlation between the 6-hour accumulated rainfall and the EnKF analysis fields at 00Z June 30 because rainfall is the direct result of previous state of the atmosphere. According to the analysis of correlation between rainfall and wind (figure not shown), there is positive correlation between rainfall and the mid-to-low level meridional/zonal wind to the west/south, and it is opposite for the high levels, which indicates the stronger the mid-low level/high level convergence/divergence and low-level jet, the larger probability of heavy rainfall after assimilation at 00Z 30.

To further verify the results of the correlation analysis, we categorize all the forecasts into “GOOD”, “WEAK” and “POOR” groups in terms of intensity and location prediction from all the ensemble members. “GOOD” include those forecasts that both forecasted intensity and location are close to observations. “WEAK” include the forecasts with good forecasted location but less rainfall. “POOR” include those forecasts with both intensity and location forecasts are not close to observations. Figure 9 shows the mean rainfall forecasted by all these three groups. Little difference can be found between “GOOD” and “WEAK” for rainfall location. The differences of the composite wind fields at 700 hPa are similar among these three groups (Fig-

ure 10(d)–(f), all generally showing a cyclonic circulation. The wind field differences between “GOOD” and “POOR” at 300 hPa (Figure 10(a)) exhibit a strong divergence with southerly winds over 12 m/s. It shows a weak divergence between “GOOD” and “WEAK” (Figure 10(b)) while large scale difference can be noticed between “WEAK” and “POOR” (Figure 10(c)). The above results suggest there is small difference of low level convergence between “GOOD” and “WEAK”, but “GOOD” has stronger divergence while “POOR” are weak for both low level convergence and high level divergence.

Vertical profile of composite reflectivity (Figure 11) shows the convection is still in the development phase at 00Z June 30. There is little difference for thermodynamic structure between these three groups. They all have a convectively unstable zone at mid-low levels. The area of high energy with pseudo equivalent potential temperature over 352 K is convectively unstable below 900 hPa and turns to stable near 600 hPa. Due to development of convection, the high convectively unstable areas almost connect to each other between the higher levels and lower levels. But for vertical velocity and reflectivity, there are significant differences between these three groups. The vertical penetration of convection for “GOOD” is above 300 hPa, it is relatively lower for “WEAK”, only reach 400 hPa, and it is even weaker for “POOR”, which only reaches near 500 hPa. Vertical penetration of convection represents the intensity of convection. At 00Z June 30, the differences of convection intensity in the initial analysis field probably are direct causes of later rainfall forecast differences. Under convectively unstable condition, the ensemble members (“GOOD”) who have a deep vertical penetration of convection with convergence at lower levels and divergence at higher levels can produce better forecast of rainfall location and intensity.

Figure 12 shows the domain averaged vertical velocity and reflectivity for the three groups. The maximum vertical

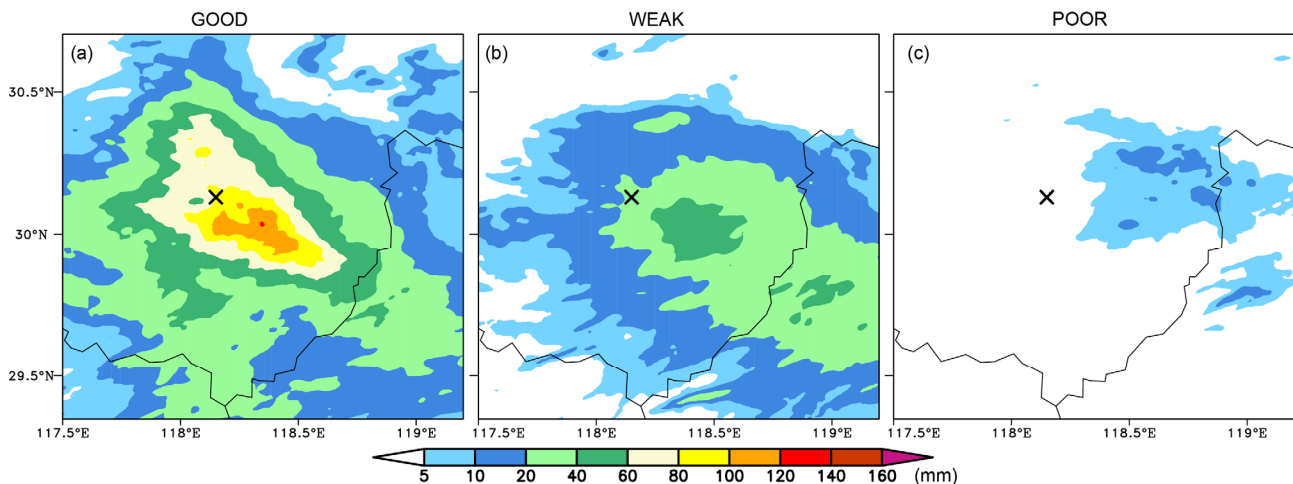


Figure 9 Composite 6-hour (00Z-06Z on June 30, 2013) accumulated rainfall for all these three groups.

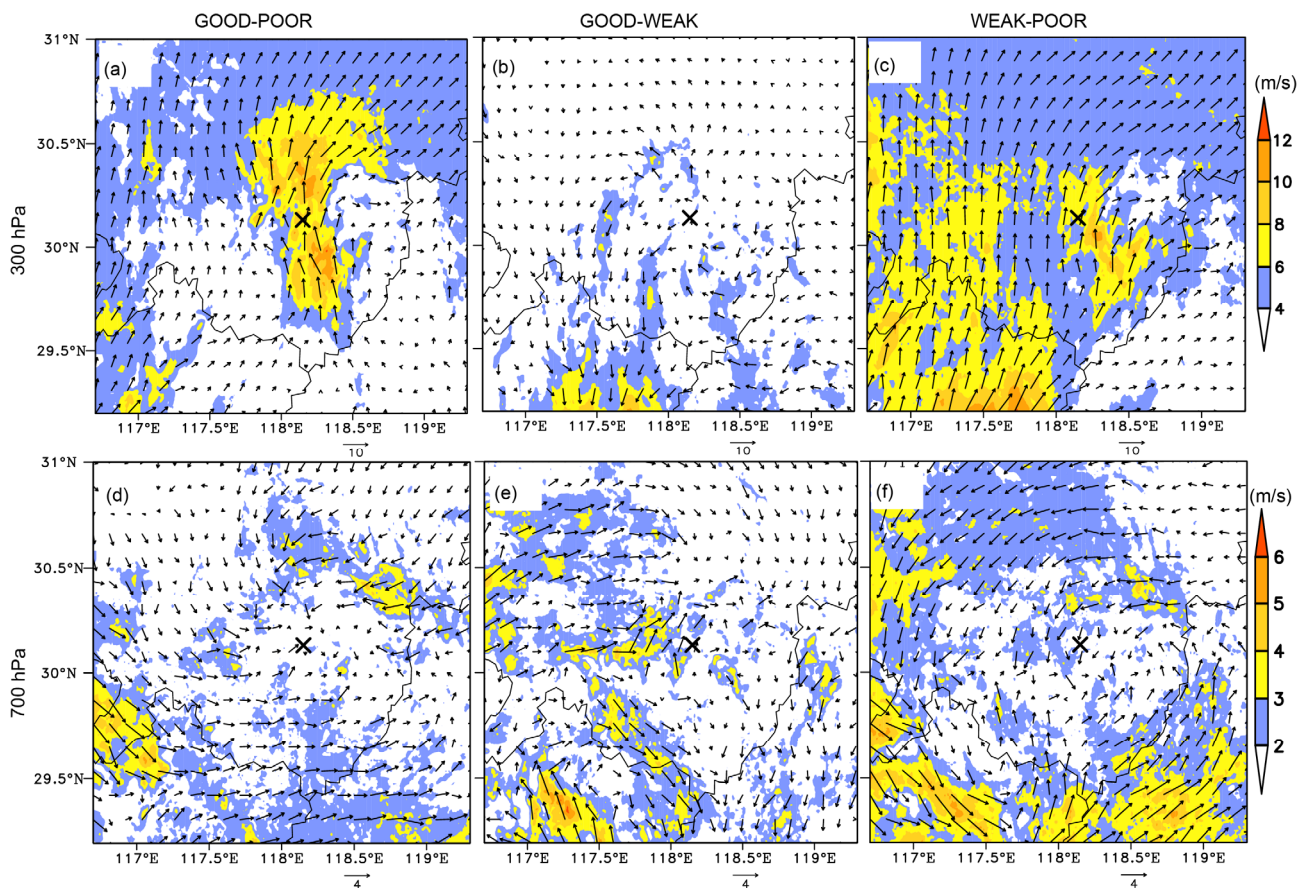


Figure 10 Difference of composite wind fields (shaded is wind speed) at 300 hPa (top) and 700 hPa (bottom) at 00Z June 30, 2013.

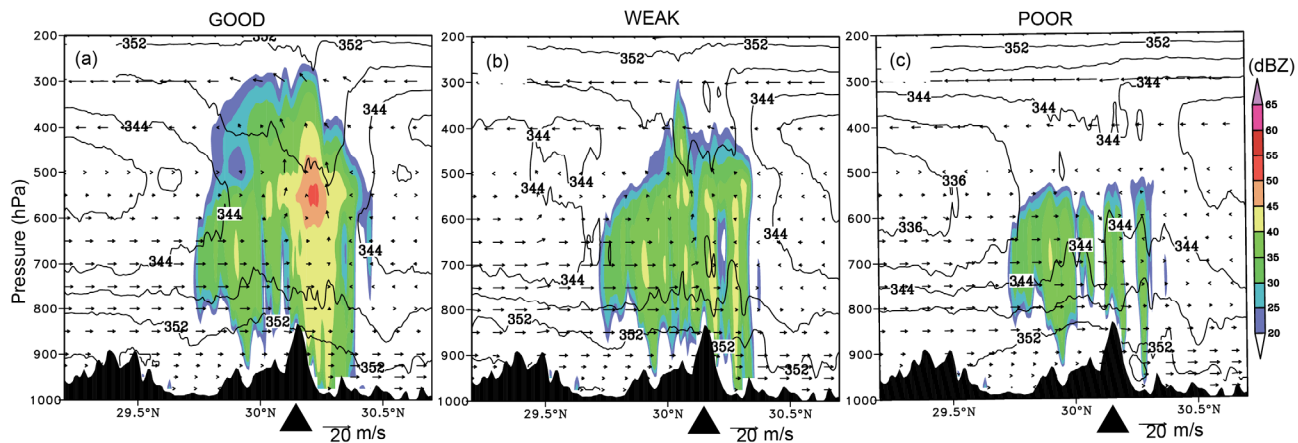


Figure 11 Vertical profile of composite reflectivity (shaded), theta-se (contour) and meridional wind (vector) along 118.2°E at 00Z June 30 in CNTL experiment. (a) GOOD-POOR (b) GOOD-WEAK (c) WEAK-POOR.

velocity is near 400 hPa for all the three groups. However, the “GOOD” has the largest vertical velocity (25 cm/s), followed by “WEAK” group (15 cm/s). The “POOR” has the weakest vertical motion (5 cm/s). As for the domain averaged reflectivity, it is larger for “GOOD” than “WEAK” and “POOR” at all levels. The echo altitude for “GOOD” (15 dBZ) is 8.6 km, much higher than “WEAK”

(7.6 km) and “POOR” (6.1 km)

As we know, mesoscale weather systems develop under favorable environmental conditions which are provided by large scale synoptic systems. A question can be raised that which factors have been changed after the assimilation of radar observations that finally lead to improved results. Based on correlation analysis of all the variables at 12Z

June 29 in domain 1 (D1), we found the correlation coefficients of mid-low level meridional wind, specific humidity and pseudo equivalent potential temperature can pass the 95% confident test. The correlations coefficients with me-

ridional winds are showed in Figure 13(a). The area with correlation coefficients larger than 0.35 is in the Jiangxi Province which is upstream of the extreme rain region. The area with strong correlation to the 850 hPa specific humidi-

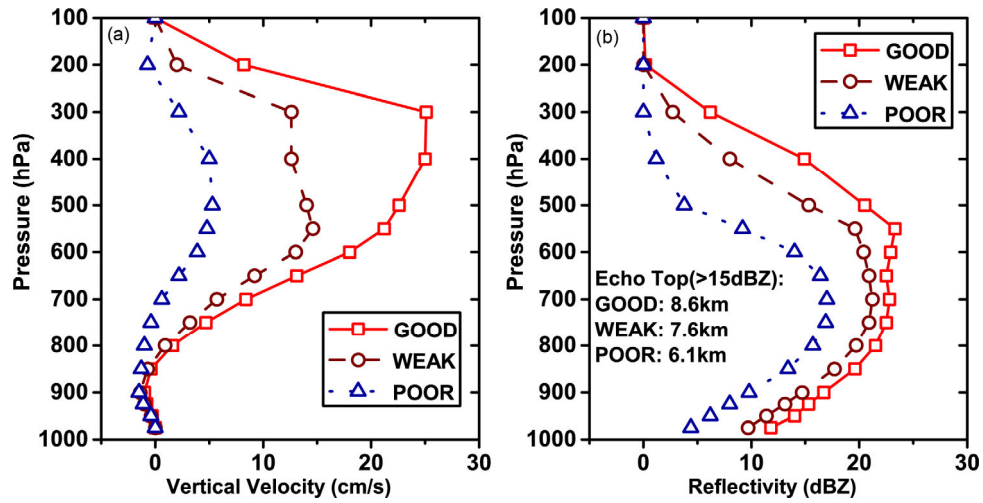


Figure 12 Vertical profile of domain averaged (a) vertical velocity and (b) reflectivity at 00Z June 30 in CNTL experiment.

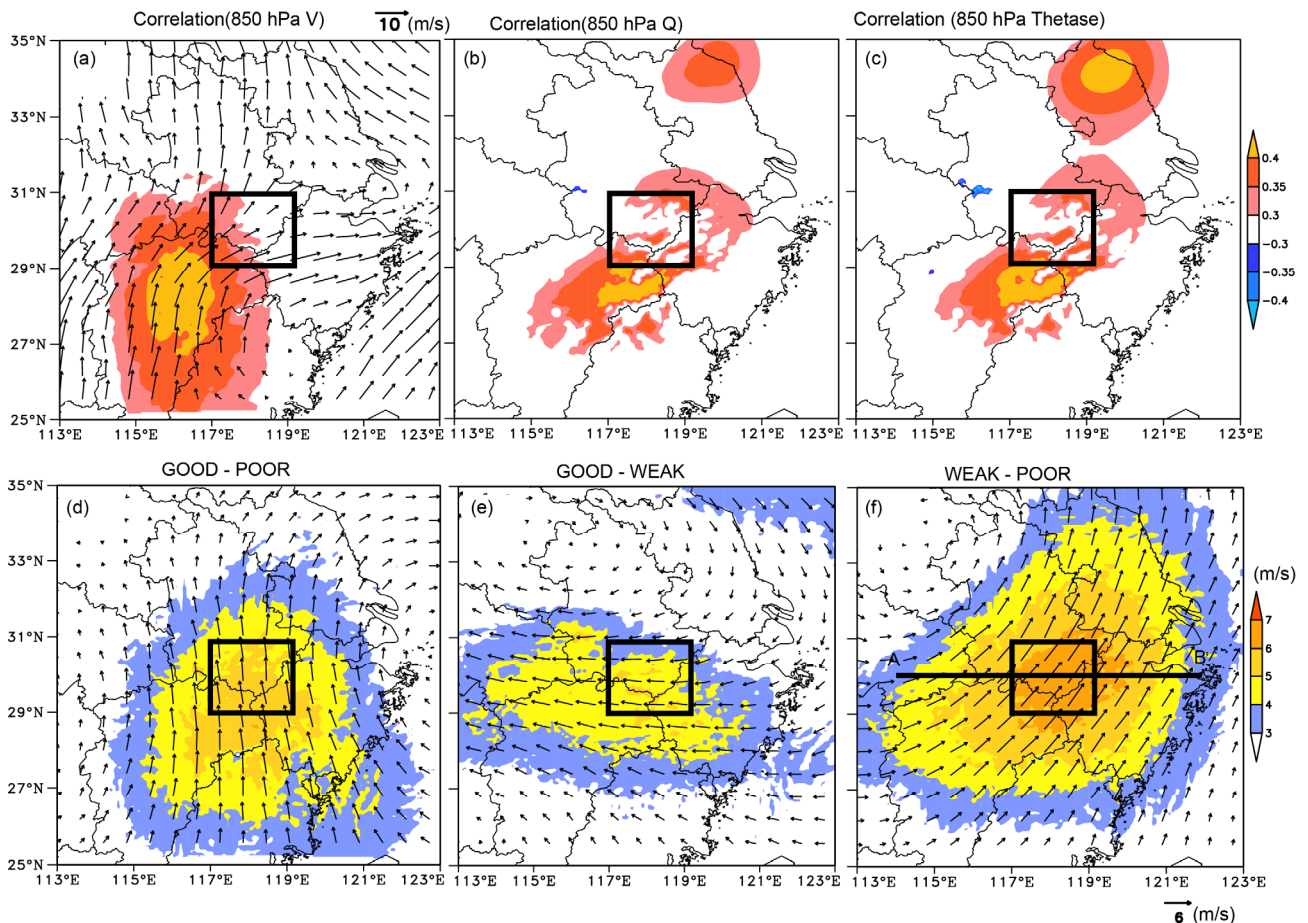


Figure 13 Correlations between 6-hour rainfall and (a) meridional wind (b) specific humidity (c) 850 hPa theta-se at 12Z June 29 in CNTL experiment. The differences between 850 hPa wind fields from three groups (GOOD, WEAK, POOR) are also showed as (d) GOOD-POOR (e) GOOD-WEAK and (f) WEAK-POOR.

ty is in the northeast of Jiangxi Province (Figure 13(b)) where is also upstream of the extreme rain region. The correlation between precipitation and the 850hPa temperature or zonal wind is small, and cannot pass 95% confidential test (figure not shown). Because pseudo equivalent potential temperature itself is dependent on temperature and specific humidity, its correlation coefficients pattern is similar to that of specific humidity (Figure 13(c)). The above results suggest the magnitude of meridional wind, specific humidity are key factors impacting the rainfall location and intensity. The difference of 850 hPa wind fields between the three groups (Figure 13(d)–(f)) showed the most significant differences are in an area centered at the heavy rainfall location, with correlation coefficients over 0.35, where southerly wind was found in the wind difference between “GOOD” and “POOR” group (Figure 13(d)), and southwesterly in the wind difference between “WEAK” and “POOR” (Figure 13(f)). The results further proved the close relationship between rainfall and upstream meridional wind strength. Low-level jet is the major carrier for energy and moisture transportation. The stronger the meridional wind, the more beneficial for forming a convective unstable area in the northeast of the low-level jet. Under the same meridional wind, the stronger the zonal wind, the more negative impact on forming that convective unstable area, like the samples in the “WEAK” group (Figure 13(e)).

Because of the differences of the upstream wind fields, after 6-hour evolution (at 18Z June 29), significant differences of dynamic and thermodynamic conditions appeared among the members in the three groups. Figure 14 showed the vertical profile of wind fields along 30N for “GOOD” members (Figure 14(a)). Southwesterly flow locates below 600 hPa, corresponding to a high energy area with pseudo equivalent potential temperature over 350 K, the area extending eastward to rainfall region, forming a convective unstable stratification, providing favorable conditions for the extreme rain. Compared with “GOOD” members, the samples in “POOR” have lower pseudo equivalent potential temperature below 600 hPa with a difference of 3–6 K (Figure 14(b)), and with a weaker convective instability and less unstable energy, and a weak southwest low-level jet, which is not favorable for deep convection. “WEAK” and “GOOD” are similar, but the pseudo equivalent potential temperature is 2 k lower than that in “GOOD” in the mid-low level (Figure 14(c)) and higher above 600 hPa, which indicates less favorable for convection development than “GOOD”. Based on all the results above, the upstream meridional wind at mid-low level is the key factor for downstream extreme rainfall. Large scale synoptic condition with strong meridional wind at mid-to-low level can provide a favorable environment for heavy rain. With EnKF assimilation of radar observations, a deep convective system

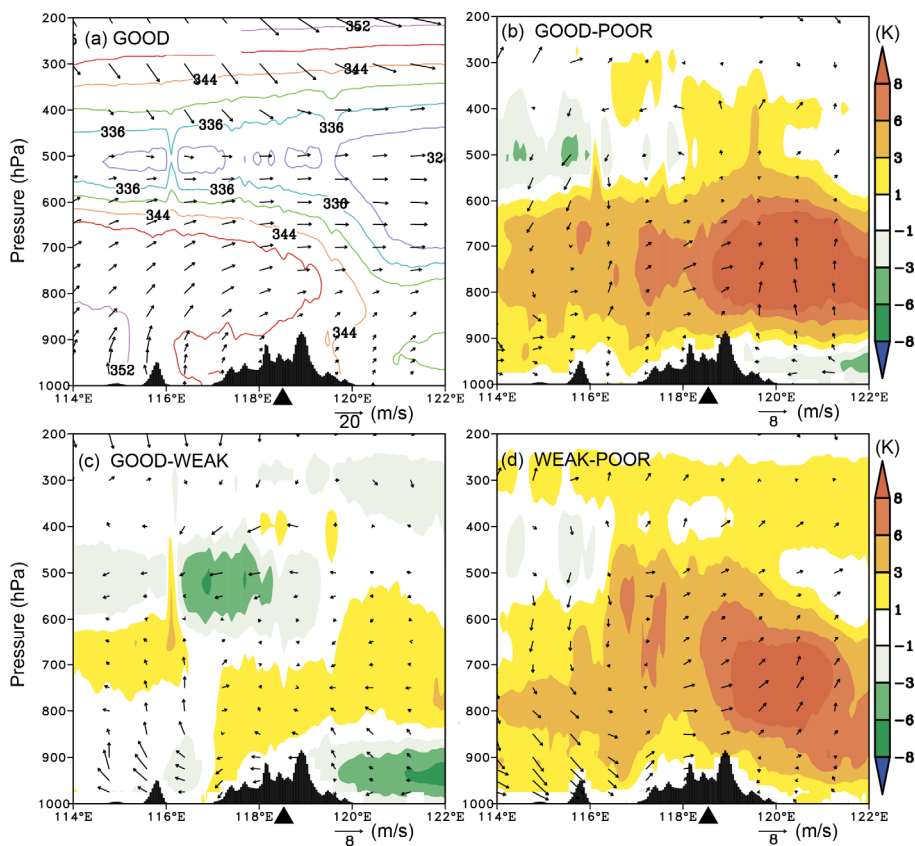


Figure 14 Vertical profile of averaged horizontal wind (vector) and theta-se (contour in (a) and shading for (b), (c) and (d)) along 30N (Line AB in Figure 11(d)) between GOOD and other groups at 18Z June 29 in CNTL experiment.

can be built up by "ingesting" high resolution information which is necessary for accurately forecast the extreme rain events like this special case.

However, even with very favorable convective unstable conditions, extreme rain cannot be predicted without assimilation of radar observations (Figure 8(a)–(c)), therefore, the initial perturbations that can represents the uncertainties of upstream mid-low level meridional wind is the key factors for EnKF assimilation of observations and followed rainfall forecast.

4.3 Sensitivity experiments

4.3.1 Different amplitude of initial perturbations experiments

As we can learn from above analysis, the rainfall forecast is closely related to initial perturbations. To examine the impact of the initial perturbation on rain forecast, we reduce the initial perturbations of the CNTL ensemble by 50% (IP0.5) and carry out the same EnKF analysis and forecast. Figure 15(a) shows result of deterministic forecast. The heaviest rainfall is located at far south of the domain, similar to the forecasted rainfall location from NoDA (Figure 7(a)). A new center of rainfall can be noticed to the southeast of radar the position of which with weaker intensity is

close to that in the CNTL experiment (Figure 5(d)). Ensemble forecasts (Figure 15(b), (c)) show 30%–40% members forecasted over 50mm rainfall in the south of Anhui Province. Though it is better than the NoDA experiment, it is as good as the CNTL experiment for rain location forecast. Analysis of 700 hPa wind fields at 00Z June 30 (Figure 6(d)) demonstrates better analyzed of meridional wind convergence compared with the NoDA experiment, with the convergence area adjusted northward, but still much different from analysis of CNTL. IP0.5 experiment suggests smaller initial perturbations possibly result in too small of the ensemble spread and background error covariance, the "ingesting" observational information decrease in the analysis, it will decrease the observation impacts on the rainfall forecast, which results the rainfall forecasts of IP0.5 are between NoDA and CNTL. For the mesoscale (convective scale) ensemble forecast, the results of NoDA and IP0.5 experiments support that (1) it is not enough by just adding perturbations for large scale initialization, and (2) the amplitude of initial perturbation is crucial even with the EnKF assimilation of radar observations.

4.3.2 EnKF cycle assimilation experiments

Previous studies showed the background error covariance is "flow-dependent", the analysis fields of which is more close

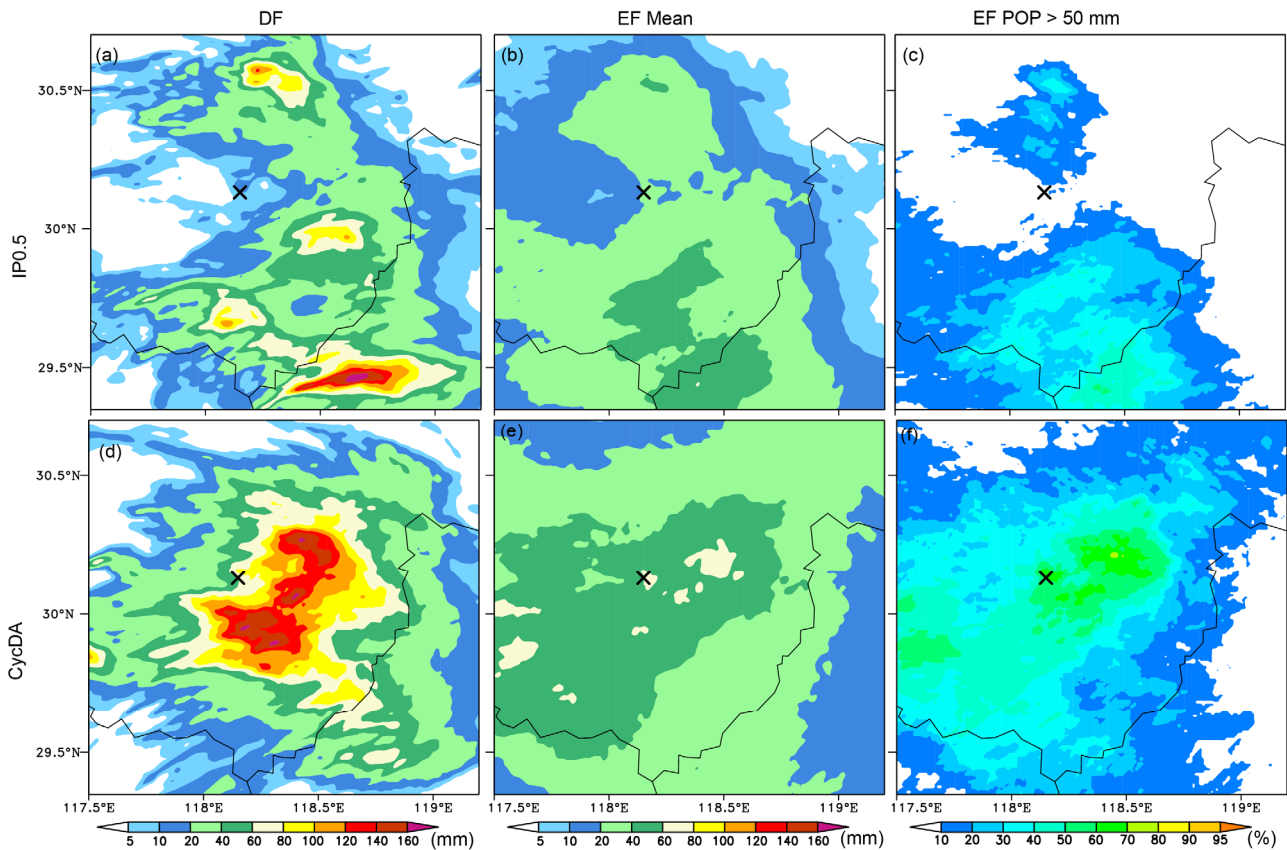


Figure 15 6-hour (from 00Z to 06Z on June 30, 2013) accumulated rainfall from deterministic forecast ((a), (d)) and ensemble mean ((b), (e)). The probability forecast for rainfall over 50mm is showed in ((c), (f)). The top panel is for IP0.5 experiment, the bottom panel is for CycDA experiment.

to real state of the atmosphere (Meng and Zhang, 2008a). In order to test if the forecast is improved with EnKF generating initial analysis fields and perturbations, we design the cycling EnKF assimilation experiment (CycDA). The initial analysis fields and perturbations at 12Z June 29 are all from EnKF results for D1 24 hours before. This analysis assimilated surface and radiosonde observations at 00Z, 06Z and 12Z. The radiosonde observations at 06Z are intensive observations conducted by China Meteorological Administration (CMA). The center of the heavy rain from deterministic forecast of CycDA (Figure 15(d)) is to the south and northeast of the radar. The location forecast is closer to observation than the CNTL experiment, and the magnitude forecast of rain is comparable with the CNTL experiment. At 00Z June 30, the meridional wind convergence zone at 700 hPa (Figure 6(c)) for CycDA and CNTL is similar in the ensemble forecasts. The forecasted ensemble mean rainfall (Figure 15(e)) and the 50mm probability forecast are both superior to the CNTL experiment. In general, the results of CycDA experiment are similar with the CNTL experiment, except for better rainfall location forecast. This experiment on the one hand suggested the sensitivity of the forecast to the initial analysis fields and perturbations, on the other hand, proved the capability of EnKF cycling assimilation for improving the forecast. The uncertainties of forecasts from

above experiments raise the question of predictability about this kind of events. Whether or not the forecast for this kind of event can be improved, needs to be answered with the analysis of intrinsic predictability for the case.

4.4 Predictability analysis

Intrinsic predictability is used to evaluate the limit of forecast by the inevitable tiny error of initial fields (Lorenz, 1969). Under the limit, no matter how small the errors of initial fields are, large uncertainties exist for future forecast. (e.g. Zhang et al. 2006a; Zhang and Sippel, 2009b; Melhauser and Zhang, 2012). To approach the subject, two more experiments were designed based on the CNTL experiment. Specifically, the difference between the ensemble members and ensemble mean was reduced to 1/2 (CNTL0.5) and 1/10 (CNTL0.1) of CNTL experiment at 00Z June 30. Then the 6-hour forecasts of these two experiments were compared with CNTL. Figure 16 shows the ensemble mean of forecasted rainfall and probability of rainfall over 50mm. We can find the ensemble mean of rainfall increase from 60mm to 80mm and probability of rainfall over 50mm increases from 50% to 80% for CNTL0.5, indicating the ensemble forecast is close to the deterministic forecast (Figure 7(d)). For CNTL0.1 experi-

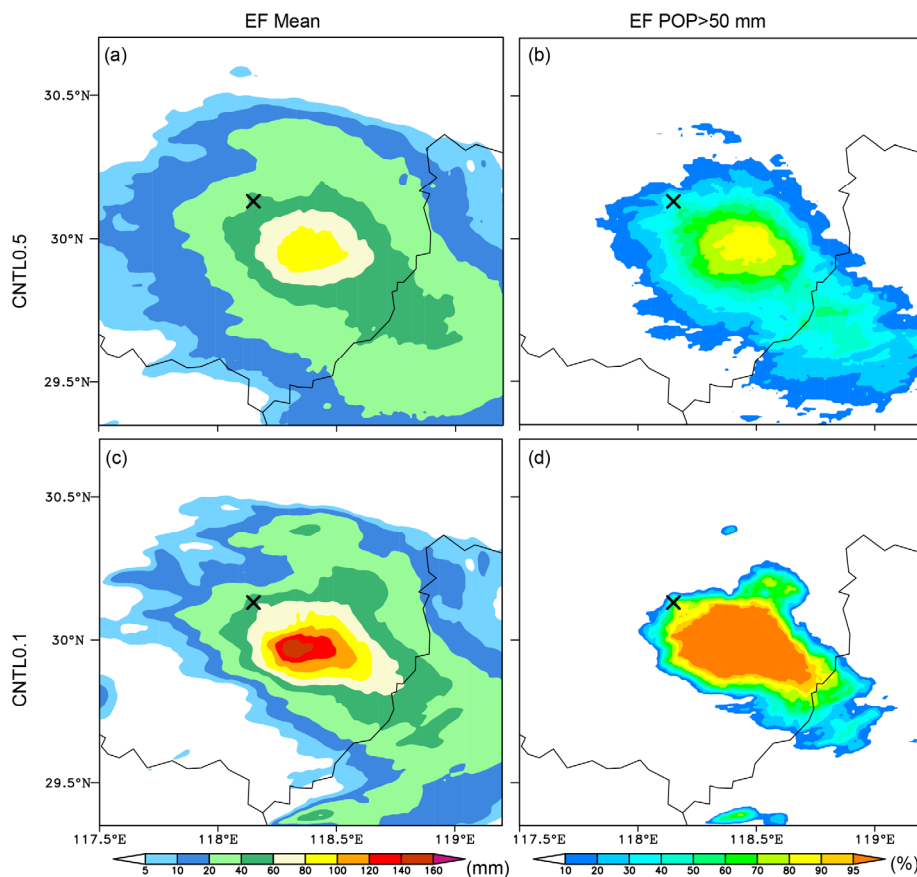


Figure 16 Comparison of rainfall of ensemble mean and probability of rainfall over 50mm at 00Z June 30, 2013 for CNTL0.5 and CNTL0.1.

ment, ensemble forecast almost identical to the deterministic forecast. The probability forecast increases to over 95%. Therefore, if the analysis of ensemble forecast is assumed to be the real state of the atmosphere, the forecasts will converge to deterministic forecast if the initial errors decrease, which indicates forecast is possibly not constrained by intrinsic predictability for 3–6 h forecasts for this case. Further improvement of forecasts can be expected by improving our numerical models, reducing the model uncertainties or providing more reliable observations by updating our observation networks. However, it is not clear what the forecast would be if we reduce the initial error to less than 10% of estimated error, and more future studies are needed for this topic.

5. Discussions and summary

In this paper, the WRF model was used to simulate a local extreme rain event occurred in the south of Anhui Province on June 30, 2013. The impact of EnKF assimilation of Doppler radar radial velocity data on WRF model forecast was analyzed. Multiple sensitivity tests have been conducted to evaluate the predictability of this extreme case with or without the assimilation of radar observations. We have following conclusions:

(1) Without EnKF assimilation of radar observations, neither deterministic forecast with single set of initial fields nor ensemble forecast with initial perturbations or multiple physics can predict the location of heavy rain accurately. With assimilation, the model continuously “ingests” high resolution observations of this weather system during the forecast, building up and adjusting the mesoscale convective system responsible for the extreme rain. As a result, both the deterministic forecast and the ensemble forecast can be improved, especially for the location forecast of the extreme rain.

(2) Whether or not a deep mesoscale convective system can be built up after data assimilation is the key to produce an accurate forecast later. The amplitude of the new mesoscale convective system is related to the large scale initial fields. Under an unstable large scale environment with high available convective energy, the upstream meridional wind convergence and moisture conditions at mid-low levels are key factors that impact the forecasts. The stronger upstream meridional wind, the more abundant moisture, which creates favorable convective unstable conditions for mesoscale convective system, and an extreme rain is more likely to happen. For the upstream area, initial perturbations of meridional wind and moisture in the mid-low levels are critical components for EnKF assimilation and the following forecast.

(3) Sensitivity tests showed predictability of this case is sensitive to realistic initial condition uncertainties. Simulation results are sensitive to EnKF generating analysis fields

which might be quite different due to different large scale initial conditions and the amplitudes of the initial perturbations. If we reduce initial perturbation of CNTL experiment by 50%, the results will be between CNTL and NoDA. Forecasts initialized by EnKF generating analysis are more close to observations. Cycling EnKF could improve the short-range forecasts for this kind of extreme rain.

(4) This event probably is not constrained by the intrinsic predictability at the 3–6 h lead time. With the current state-of-art EnKF assimilation method, further improvement of forecasts can be expected by improving our numerical models, reducing the model uncertainties or providing more reliable observations by updating our observation networks.

In order to analyze the predictability of this case, the experiment with the best result is set as the control experiment. This experiment only assimilates the lowest elevation angles radar radial velocity observations. Theoretically, the initial condition should be more close to reality when assimilate all the available angles of radar observations. While in this case, the deterministic forecast with assimilation all the angles of radar observations are not as good as the control experiment. Statistically, forecast error covariance in deterministic forecast is the most optimal, but it probably does not reflect the reality. The forecast of ensemble member 6, 18 and 20 (figure not shown) are very close to the control experiment (Figure 8(d)–(f)), which is also support the uncertainty of the forecast. For such kind of case, ensemble forecast is superior to single deterministic forecast. Regarding to the dynamic factors responsible for this extreme rain, in addition to the low-level jet and convergence zone mentioned previously, complex terrain possibly also plays a role in this event. We will conduct some other sensitivity experiments in the future studies. Because EnKF assimilation requires continuous multiple time observations, which is not available for the sudden local extreme rain event, it can only apply to some specific cases. The case discussed in this paper is very special—it happened on the edge of subtropical high with complex terrain and the radar is located at an elevation of 1800 m (near 850 hPa). Therefore, analysis of more cases are needed to verify the results from this paper.

Acknowledgements *The authors would like to thank the two anonymous referees for comments that improved the quality of the paper.*

References

- Aksoy A, Dowell D C, Snyder C. 2009. A multi-case comparative assessment of the ensemble Kalman filter for assimilation of radar observations. Part I: Storm-scale analyses. *Mon Weather Rev*, 137: 1805–1824
- Aksoy A, Dowell D C, Snyder C. 2010. A multi-case comparative assessment of the ensemble Kalman filter for assimilation of radar observations. Part II: Short-range ensemble forecasts. *Mon Weather Rev*, 138: 1273–1292
- Barker D M, Huang W, Guo Y R, Bourgeois A J, Xiao Q N. 2004. A three-dimensional variational data assimilation system for MM5: Implementation and initial results. *Mon Weather Rev*, 132: 897–914

- Bei N F, Zhang F Q. 2007. Mesoscale predictability of the torrential rainfall along the mei-yu front of China. *Q J R Meteorol Soc*, 133: 83–99
- Dowell D C, Zhang F Q, Wicker L J, Snyder C, Crook A. 2004. Wind and thermodynamic retrievals in the 17 May 1981 Arcadia, Oklahoma, supercell: Ensemble Kalman filter experiments. *Mon Weather Rev*, 132: 1982–2005
- Hong S Y, Dudhia J, Chen S H. 2004. A revised approach to ice-microphysical processes for the bulk parameterization of cloud and precipitation. *Mon Weather Rev*, 132: 103–120
- Lan W R, Zhu J, Xue M, Gao J D, Lei T. 2010a. Storm-scale ensemble Kalman filter data assimilation experiments using simulated Doppler radar data. Part I: Perfect model tests (in Chinese). *Chin J Atmos Sci*, 34: 640–652
- Lan W R, Zhu J, Xue M, Lei T, Gao J D. 2010b. Storm-scale ensemble Kalman filter data assimilation experiments using simulated Doppler radar data. Part II: Imperfect model tests (in Chinese). *Chin J Atmos Sci*, 34: 737–753
- Liu J Y, Tan Z M. 2009. Mesoscale predictability of Mei-yu heavy rainfall. *Adv Atmos Sci*, 26: 438–450
- Lorenz. 1969. Atmospheric predictability as revealed by naturally occurring analogues. *J Atmos Sci*, 26: 636–646
- Melhauser C, Zhang F Q. 2012. Practical and intrinsic predictability of severe and convective weather at the mesoscales. *J Atmos Sci*, 69: 3350–3371
- Meng Z Y, Zhang F Q. 2007. Test of an ensemble Kalman filter for mesoscale and regional-scale data assimilation. Part II: Imperfect-model experiments. *Mon Weather Rev*, 135: 1403–1423
- Meng Z Y, Zhang F Q. 2008a. Test of an ensemble Kalman filter for mesoscale and regional-scale data assimilation. Part III: Comparison with 3DVAR in a real-data case study. *Mon Weather Rev*, 136: 522–540
- Meng Z Y, Zhang F Q. 2008b. Test of an ensemble Kalman filter for mesoscale and regional-scale data assimilation. Part IV: Performance over a warm-season month of June 2003. *Mon Weather Rev*, 136: 3671–3682
- Min J Z, Chen J, Wang S Z, Bao Y S. 2011. The tests of WRF-EnSRF data assimilation system and its applications in storm-scale events (in Chinese). *Chin J Meteorol Sci*, 31: 135–144
- Noh Y, Cheon W G, Hong S Y. 2003. Improvement of the K-profile model for the planetary boundary layer based on large eddy simulation data. *Bound-Layer Meteorol*, 107: 401–427
- Schumacher R S, Johnson R H. 2005. Organization and environmental properties of extreme-rain-producing mesoscale convective systems. *Mon Weather Rev*, 133: 961–976
- Schumacher R S, Johnson R H. 2006. Characteristics of U.S. extreme rain events during 1999–2003. *Weather Forecast*, 21: 69–85
- Sippel J A, Braun S A, Shie C L. 2011. Environmental influences on the strength of Tropical Storm Debby (2006). *J Atmos Sci*, 68: 2557–2581
- Sippel J A, Zhang F Q. 2008. A probabilistic analysis of the dynamics and predictability of tropical cyclogenesis. *J Atmos Sci*, 65: 3440–3459
- Sippel J A, Zhang F Q. 2010. Factors affecting the predictability of Hurricane Humberto (2007). *J Atmos Sci*, 67: 1759–1778
- Skamarock W C, Klemp J B, Dudhia J, Gill D O, Barker D M, Duda M G, Huang X Y, Wang W, Powers J R. 2008. A description of the Advanced Research WRF version 3. NCAR Tech Note 4751STR, 113
- Snyder C, Zhang F Q. 2003. Tests of an ensemble Kalman filter for convective-scale data assimilation. *Mon Weather Rev*, 131: 1663–1677
- Tippett M K, Anderson J L, Bishop C H, Hamill T M, Whitaker J S. 2003. Ensemble square root filters. *Mon Weather Rev*, 131: 1485–1490
- Tong M, Xue M. 2005. Ensemble Kalman filter assimilation of Doppler radar data with a compressible nonhydrostatic model: OSS experiments. *Mon Weather Rev*, 133: 1789–1807
- Xu X Y, Liu L P, Zheng G G. 2006. Numerical Experiment of Assimilation of Doppler Radar Data with an Ensemble Kalman Filter (in Chinese). *Chin J Atmos Sci*, 30: 712–728
- Xue M, Tong M, Droegemeier K K. 2006. An OSSE framework based on the ensemble square-root Kalman filter for evaluating impact of data from radar networks on thunderstorm analysis and forecast. *J Atmos Ocean Technol*, 23: 46–66
- Weng Y H, Zhang F. 2012. Assimilating Airborne Doppler Radar Observations with an Ensemble Kalman Filter for Convection-Permitting Hurricane Initialization and Prediction: Katrina (2005). *Mon Weather Rev*, 140: 841–859
- Whitaker J S, Hamill T M. 2002. Ensemble data assimilation without perturbed observations. *Mon Weather Rev*, 130: 1913–1924
- Zhang F Q, Snyder C, Rotunno R. 2004. Tests of an ensemble Kalman filter for convective-scale data assimilation: Impact of initial estimate and observations. *Mon Weather Rev*, 132: 1238–1253
- Zhang F Q, Odins A M, Nielsen-Gammon J W. 2006a. Mesoscale predictability of an extreme warm-season precipitation event. *Weather Forecast*, 21: 149–166
- Zhang F Q, Meng Z Y, Aksoy A. 2006b. Test of an ensemble Kalman filter for mesoscale and regional-scale data assimilation. Part I: Perfect-model experiments. *Mon Weather Rev*, 134: 722–736
- Zhang F Q, Weng Y H, Sippel A J, Meng Z Y. 2009a. Convection-permitting hurricane initialization and prediction through assimilation of Doppler radar observations with an ensemble Kalman filter: Humberto (2007). *Mon Weather Rev*, 137: 2105–2125
- Zhang F Q, Sippel J A. 2009b. Effects of moist convection on hurricane predictability. *J Atmos Sci*, 66: 1944–1961
- Zhang F Q, Weng Y H. 2015. Modernizing the prediction of hurricane intensity and associated hazards: A five-year real-time forecast experiment concluded by superstorm Sandy (2012). *Bull Amer Meteorol Soc*, 96: 25–33
- Zhang X L, Yu R, Du M Y. 2014. Evolution pattern of short-time intense precipitation-producing systems associated with Meiyu front (in Chinese). *Chin J Atmos Sci*, 38: 770–781
- Zhu B L, Lin W T, Zhang Y. 2009. Impact s of initial perturbations on prediction of a heavy rain in South China (in Chinese). *Chin J Atmos Sci*, 33: 1333–1347